

Small-Angle Neutron Scattering Investigation of Topological Constraints and Tube Deformation in Networks

E. Straube

Martin-Luther-Universität Halle-Wittenberg, Fachbereich Physik, D-06099 Halle, Germany

V. Urban, W. Pyckhout-Hintzen, and D. Richter

Forschungszentrum Jülich, Institut für Festkörperforschung, Postfach 1913, D-52425 Jülich, Germany

C. J. Glinka

National Institute of Standards and Technology, Gaithersburg, Maryland 20899

(Received 25 January 1995)

The effect of topological constraints on the microscopic deformation of network chains in a statistically cross-linked rubber under uniaxial deformation is addressed by small-angle neutron scattering (SANS) on labeled paths in a network. The observed SANS patterns exhibit a pronounced transition from elliptical to lozengic shapes. Within a tube approach for the constraining potential the scattering function is calculated in the 2D detector plane. Excellent agreement between the statistical mechanical model and the experimental results is obtained.

PACS numbers: 61.41.+e, 61.12.Ex, 83.80.Dr

The microscopic structure and dynamics of entangled polymer melts and networks have been a focus of attention ever since the creation of the reptation model [1,2] in the early seventies. Being a very elegant mean-field description this model treats the entanglements of mutually interpenetrating polymer chains by the assumption of a confinement of chain segments inside a soft tube along the chain's profile. The existence of the tube is now well accepted, and direct observations of the corresponding length scale d_0 have been reported examining the dynamics of melts by neutron-spin-echo methods [3,4]. Topological interactions giving rise to the tube constraints in the melt have also a decisive importance for the chain conformations that may be achieved in networks. Intuitively it may be assumed that the constraints deform affinely with the macroscopic deformation λ [5–7]. This assumption leads to the famous Mooney-Rivlin equation for the stress-strain relations in rubbers. Later Heinrich and Straube [8,9] approximated the tube constraints within a self-consistent mean-field approach by a harmonic potential and determined the strength and the deformation behavior of the confining potential. Their approach predicts for a deformed network with main axis deformation ratios λ_μ a pronounced nonaffine deformation of the equilibrium tube diameter d_0 as

$$d_\mu = d_0 \lambda_\mu^\nu, \quad (1)$$

with $\nu = \frac{1}{2}$. Mechanical investigations are in agreement with the exponent $\nu = \frac{1}{2}$ but are too insensitive to discern between an affine behavior $\nu = 1$ and the theoretical prediction [10,11]. Small-angle neutron scattering (SANS) is the proper technique to test the assumptions of the model independently and to provide a profound experimental background for the parameters of the model. In this

work we present 2D SANS data on labeled chains cross-linked within a network for different degrees of strain. Depending on strain the 2D patterns exhibit a significant transition from the expected ellipsoidal to a lozengic shape. On the basis of the mean-field tube model we calculated the 2D scattering function as a function of strain. Only for a nonaffine constraint deformation with $\nu = \frac{1}{2}$ the theoretical iso-intensity contour lines exhibit the same ellipsoidal-lozengic transition. Furthermore, the magnitude of the determined equilibrium tube diameter d_0 agrees well with results from neutron-spin-echo experiments [3,4].

The ellipsoid-lozenge transition was considered in literature only scarcely until now and a clear picture could not be presented. Systematic studies of network formation in relation to the appearance of lozenges in melts and rubbers were performed by Boue *et al.* [12] and Zielinski [13]. The weaker anisotropy in the parallel direction, however, could not be explained in terms of a rubber elastic theory, and a link rather than the butterfly patterns was proposed. des Cloizeaux [14] treated entanglements as fixed, affinely deforming stress points and chain segments as Brownian. He obtained a tendency to lozengic patterns, but the lozengic shape is very weak and no fit of experimental data was reported.

The experiments were carried out on partially labeled polyisoprene (PI) networks. The polymers were prepared by anionic polymerization of the protonated and deuterated (99%) monomers in hexane by standard high-vacuum techniques at ambient temperature. Molecular weights M_w and weight distributions were measured independently by low angle laser light scattering and size exclusion chromatography. Networks were prepared by mixing appropriate amounts of *d*-PI (10%, $M_w = 207\,000$ g/mol, $M_w/M_n = 1.015$) and *h*-PI (90%,

$M_w = 131\,000$ g/mol, $M_w/M_n = 1.015$) and a stoichiometric amount of the cross-linker, Dicumylperoxide in Tetrahydrofuran. The solvent was evaporated under vacuum. Cross-linking proceeded in bulk at 165°C for 4 h. Stress-strain plots were recorded with strain velocity about $9.8 \times 10^{-5} \text{ s}^{-1}$. A network chain mass of $M_c = 9200 \pm 500$ g/mol between cross-links was obtained in agreement with swelling data in cyclohexane ($M_c = 9700$ g/mol). The soluble part was extracted in the same solvent and the gel fraction was determined from the dry-weight difference of the rubber before and after the extraction procedure. The corresponding gel fraction was $\phi_{\text{gel}} = 0.97 \pm 0.02$.

SANS data were recorded using the NG-7 SANS instrument at the National Institute of Standards and Technology, Gaithersburg, with a neutron wavelength of $\lambda_N = 6.0 \text{ \AA}$ with wavelength spread ca. 9% and converted to absolute scale by means of a calibrated silica standard. The measurement range was 0.003 to 0.09 \AA^{-1} in terms of the scattering vector $\mathbf{Q} = (4\pi/\lambda_N) \sin(\theta/2)$ with θ the scattering angle. The incoherent background was measured separately from a fully unlabeled network of comparable cross-link density and subtracted. Macroscopic strains were determined within 5% accuracy from a grid of marks on the sample. The experimental length-to-width ratios upon straining were in absolute agreement with an affine sample deformation. Typical isointensity curves at different strains are shown in Fig. 1. The radius of gyration R_g in the isotropic state is $142 \pm 2 \text{ \AA}$ and is in accordance with θ -temperature dimensions. No influence of the cross-linking process on the chain dimensions was found. The scattering at $Q = 0$ yields the same molecular

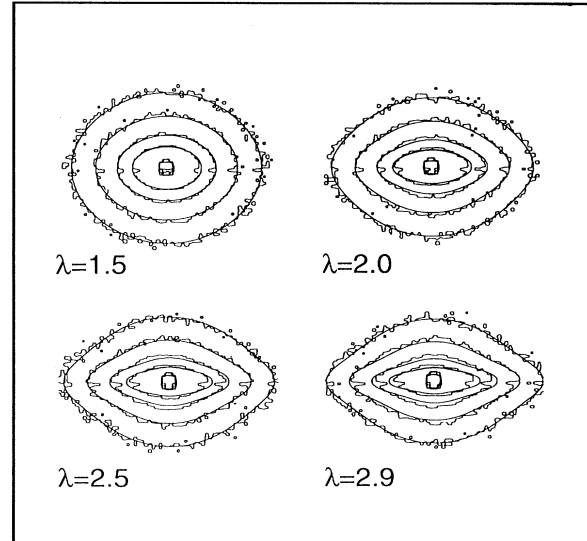


FIG. 1. Experimental SANS pattern from deformed networks and best-fit curves for strains $\lambda = 1.5, 2.0, 2.5,$ and 2.9 . Outer limits of the principal axes in both directions correspond to $QR_g = 13$. The stretching direction is vertical.

weight as light scattering from dilute solutions in hexane and Flory-Huggins corrections for the isotopic mixture are unnecessary.

Within the framework of the tube model [5] the conformations of the labeled path can be described by the following conditional distribution function, describing the actual configurations $\mathbf{R}(s)$ of a network chain for a given mean configuration $\hat{\mathbf{R}}(s)$:

$$p(\mathbf{R}(s) | \hat{\mathbf{R}}(s)) \sim \exp\left\{-3/2l_{\text{st}} \int_0^L ds [\partial \mathbf{R}(s)/\partial s]^2 - \sum_{\mu} w_{\mu}^2 \int_0^L ds [R_{\mu}(s) - \lambda_{\mu} \hat{R}_{\mu}(s)]^2\right\}. \quad (2)$$

The first part of the exponential in Eq. (2) is the Wiener integral and describes the entropy of a free random walk chain, whereas the second term models the confinement in terms of an entropic potential. The w_{μ} are the parameters of this harmonic confining potential. The index $\mu = x, y, z$ denotes the main axis directions of the deformation tensor with components λ_{μ} and assuming incompressibility, l_{st} is the statistical (Kuhn's) segment length, and L is the contour length of the labeled path, s being the arclength variable.

Using the Warner-Edwards [15] approach as the theoretical basis for the calculation of the form factor of a labeled path in a network, the chain model of Eq. (2) gives

$$S(\mathbf{Q}, \lambda) = 2 \int_0^1 d\eta \int_0^{\eta} d\eta' \prod_{\mu} \exp\left\{-(Z_{\mu} \lambda_{\mu})^2 (\eta - \eta') - Z_{\mu}^2 (1 - \lambda_{\mu}^2) \frac{d_{\mu}^2}{2\sqrt{6} R_g^2} \left[1 - \exp\left(-\frac{\eta - \eta'}{d_{\mu}^2/2\sqrt{6} R_g^2}\right)\right]\right\}, \quad (3)$$

which factorizes in the principal axes. The double integral in Eq. (3) runs over dimensionless chain length coordinates η and η' . The scattering from an affinely deformed chain is contained in the first term of Eq. (3), whereas the second term follows from the confinement term in Eq. (2). For convenience instead of potential parameters now deformed tube diameters d_{μ} are introduced [11].

R_g is the radius of gyration of the labeled path in the undeformed isotropic state and $Z_{\mu} = Q_{\mu} R_g$ is a component

of the reduced scattering wave vector in the main axis system of the deformation tensor. d_{μ} is defined as in Eq. (1) and depends sensitively on λ_{μ} . For $\lambda = 1$ the Debye curve is retrieved.

The left part of Fig. 2 shows the contour plots of experimental data together with the best fit for a macroscopic extension ratio $\lambda = 2.93$ for three values of the power-law exponent ν , i.e., $\nu = 0$, $\nu = \frac{1}{2}$, and $\nu = 1$. Considerable differences are noticed in varying ν and

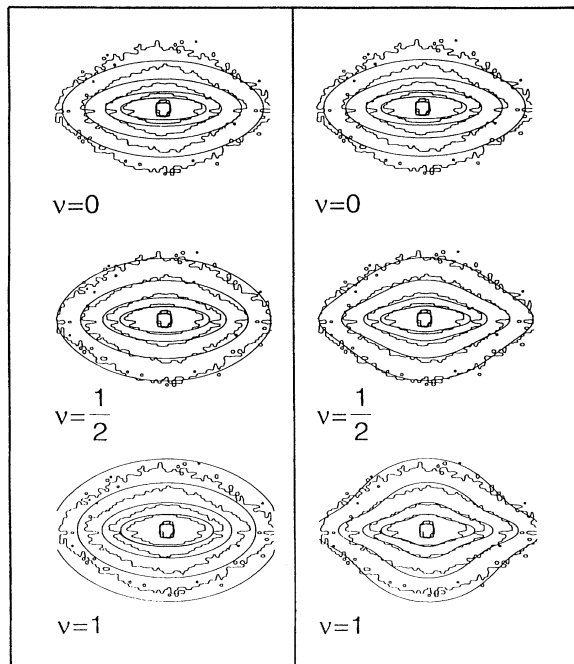


FIG. 2. $S(Q_x, Q_y, \lambda)$ as a function of ν for the strain $\lambda = 2.93$. Strain direction and outer limits of principal axes as in Fig. 1. Original form factor with axis separability for fluctuation part \tilde{d}_μ (left); modified form factor with effective fluctuation parameter \tilde{d}_ϕ (right) as defined in text.

only with $\nu = \frac{1}{2}$ the fit can be accepted. Here, the scattering intensity along both principal axes of the ellipse is approximated quite well, whereas for off-axis directions clear discrepancies remain. Both $\nu = 0$ and 1 fits are unable to describe the main directions at the same time with the same parameters. However, the result for $\nu = \frac{1}{2}$ shows that the separability of axes does not seem to work well for the fluctuation part of the form factor and modifications of the angular dependence of the restoring potential are necessary.

Equation (3) was obtained expressing the restrictions on the chain configurations due to topological constraints and cross-links by harmonic pseudopotentials as in Eq. (2) by a sum over contributions from the main axes. In this approximation the exponent in Eq. (3) consists of a sum of products of the main axis components of the scattering vector, the deformation ratio, and the mean square fluctuations. The experimental results in Fig. 2 show a different behavior. It can be obtained introducing a modified restoring potential. If one defines ϕ as the angle between the stretching direction and the scattering vector in the scattering plane, the effective deformation ratio along this direction is obtained strictly from

$$\lambda_\phi^2 = \lambda_\parallel^2 \cos^2 \phi + \lambda_\perp^2 \sin^2 \phi. \quad (4)$$

Using this effective deformation ratio λ_ϕ as measured for the local deformation in the vicinity of a restricted chain the mean square fluctuation probed by the corresponding

scattering vector is then given by

$$d_\phi^2 = d_0^2 \lambda_\phi^{2\nu}. \quad (5)$$

We have then to replace d_μ in Eq. (3) by the effective direction dependent value d_ϕ and for $S(\mathbf{Q}, \lambda)$ a modified constraint contribution results. Because of this new ϕ dependence of the fluctuation range, the presented form factor is nonfactorizable.

The introduction of such a form of the confining potential is still compatible with the original Warner-Edwards approach because only the harmonic dependence of the confining potential is important for the result.

The right part of Fig. 2 shows the contour plots of experimental data together with the best fit with Eq. (5) for the extension ratio $\lambda = 2.93$ and the three values $\nu = 0$, $\nu = \frac{1}{2}$, and $\nu = 1$. The $\nu = 0$ case is again shown and is of course identical with the original form factor. An affine deformation of the tube, $\nu = 1$, can be excluded on the basis of the pronounced different ϕ dependence and on the lack of agreement parallel to the strain axis, whereas the case $\nu = \frac{1}{2}$ shows almost perfect agreement.

After the modification Eq. (3) has the important property that for the scattering direction with

$$\sum_\mu Z_\mu^2 \lambda_\mu^2 = \sum_\mu Z_\mu^2 \quad (6)$$

the second term in the exponent vanishes, and therefore the scattering is identical with the scattering from the undeformed sample which also has been recognized by Boue [16]. Following this idea we have determined the actual microscopic deformation on the chain level by subtracting the data for the reference isotropic state from the anisotropic data. The microscopic strain component λ_\parallel follows from simply measuring the isotropy angle ϕ^* between the stretching axis and zero difference intensity lines and then solving Eq. (6) for λ_\parallel assuming volume conservation ($\lambda_\perp = 1/\sqrt{\lambda_\parallel}$). It results in

$$\lambda_\parallel = -\frac{1}{2} + \sqrt{\frac{1}{4} + \tan^2 \phi^*}. \quad (7)$$

In Fig. 3 the contour plot of the difference of scattering intensity again for the stretched sample with $\lambda = 2.93$ and the isotropic sample is shown. The isointensity line for vanishing differences yields the value $\phi^* = 73^\circ \pm 1^\circ$ and a corresponding value $\lambda_\parallel = 2.8 \pm 0.3$ in good agreement with the macroscopic extension ratio of the sample. The theoretical straight line is the vanishing difference of both best-fit functions. It is noted that the original model of Eq. (3) with axis separability does not comply with the experimentally obtained straight line. The uncertainty in deriving the microscopic strain in this way is estimated to be better than 10% and permits a quantitative check of the type of deformation, even at large \mathbf{Q} vectors. Within experimental error the effect of chain ends which may not be deformed but do contribute to the form factor can be neglected here and affinity in the deformation found. Figure 1 show the scattering data for $2 < QR_g < 13$ for all measured extension ratios and their respective fits

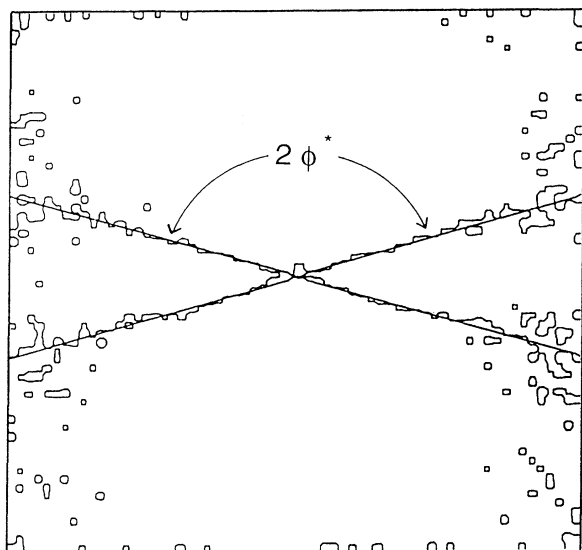


FIG. 3. Isointensity lines for vanishing difference between isotropic and anisotropic data for a macroscopic strain $\lambda = 2.9$. Straight lines represent the difference between the best-fit curves. ϕ^* is the isotropy angle as defined in Eq. (7).

using Eq. (3) and one single value $d_0 = 44 \pm 2 \text{ \AA}$ and $\nu = \frac{1}{2}$. The value for the tube diameter is comparable to results from neutron-spin-echo experiments and plateau moduli for polyisoprene melts ($d_0 \approx 51 \text{ \AA}$) [4] and agrees also reasonably with $d_0 = 37 \pm 3 \text{ \AA}$ obtained from the stress-strain data of the same network. This slightly smaller value reflects the reduced fluctuations at cross-link positions. The confinement parameter is constant over the explored deformation ratio range and demonstrates that the strain dependence is therefore correctly taken into account. The agreement with the SANS data in the whole Q range is almost perfect and proves that the applied tube model can indeed give a consistent description of the statistical mechanics of rubberelastic networks.

Consequently, we conclude that the tube model for entangled systems with predominant constraint contributions and their proposed simple nonaffine deformation dependences gives a natural explanation for the occurring microscopic deformations in the plane spanned by λ_{\parallel} and λ_{\perp} and for the appearance of lozengic structures in the scattering patterns of deformed networks.

The authors thank M. Hintzen for the polymer characterizations and A. Gabler for the stress-strain work. The providence of the beam time at the National Institute of Standards and Technology is greatly acknowledged.

-
- [1] P.G. de Gennes, *J. Chem. Phys.* **55**, 572 (1971).
 - [2] M. Doi and S.F. Edwards, *The Theory of Polymer Dynamics* (Clarendon, Oxford, 1986).
 - [3] D. Richter, B. Farago, L.J. Fetters, J. S. Huang, B. Ewen, and C. Lartigue, *Phys. Rev. Lett.* **64**, 1389 (1990).
 - [4] D. Richter, R. Butera, L. J. Fetters, J. S. Huang, B. Farago, and B. Ewen, *Macromolecules* **25**, 6156 (1992).
 - [5] R.T. Deam and S.F. Edwards, *Philos. Trans. R. Soc. London A* **280**, 543 (1976).
 - [6] P.G. de Gennes, *J. Phys. (Paris), Lett.* **5**, 133 (1974).
 - [7] S.F. Edwards and T.A. Vilgis, *Rep. Prog. Phys.* **51**, 243 (1988).
 - [8] G. Heinrich and E. Straube, *Acta Polym.* **34**, 589 (1983); **35**, 115 (1984).
 - [9] G. Heinrich and E. Straube, *Polym. Bull.* **17**, 247 (1987); **17**, 255 (1987).
 - [10] D. Matzen and E. Straube, *Colloid Polym. Sci.* **270**, 1 (1992).
 - [11] G. Heinrich, E. Straube, and G. Helms, *Adv. Polym. Sci.* **85**, 33 (1988).
 - [12] F. Boue, J. Bastide, M. Buzier, A. Lapp, J. Herz, and T. A. Vilgis, *Colloid Polym. Sci.* **269**, 195 (1991).
 - [13] F. Zielinski, Ph.D. thesis, University Pierre et Marie Curie, Paris VI, 1991.
 - [14] J. des Cloizeaux, *J. Phys. I (France)* **4**, 539 (1993).
 - [15] M. Warner and S.F. Edwards, *J. Phys. A* **11**, 1649 (1978).
 - [16] F. Boue, *Adv. Polym. Sci.* **82**, 47 (1987).